NASA CR-158,111

NASA-CR-158111
19790008680

A Reproduced Copy

OF

Reproduced for NASA

by the

NASA Scientific and Technical Information Facility

(NASA-CR-158111) THE ANALYSIS OF PROPELLERS INCLUDING INTERACTION EFFECTS (Pennsylvania State Univ.) 38 p HC A03/MF A01 CSCL 02A

N79-16851

Unclas
G3/07 14069

The Analysis of Propellers Including Interaction Effects*

B. W. McCormick
Professor and Head
Department of Aerospace Engineering
The Pennsylvania State University

A. S. Aljabri
Graduate Assistant
Department of Aerospace Engineering
The Pennsylvania State University

S. J. Jumper
Graduate Assistant
Department of Aerospace Engineering
The Pennsylvania State University

Z. N. Martinovic
Graduate Assistant
Department of Aerospace Engineering
The Pennsylvania State University

*This work was performed under NASA Grant NSG 1308

N79-16851

ABSTRACT

Analytical and experimental studies have been undertaken on propellers operating in the unsteady flow field produced by interaction effects due to the fuselage, wing, and nacelles. Methods have been developed and verified experimentally for determining the velocity field in which a propeller operates as well as its aerodynamic and dynamic response to this unsteady environment. Methods are presented for predicting the net thrust of a propeller-wing-body combination as well as the unsteady thrust and torque acting on the propeller. Sample calculations as well as wind tunnel and flight test results are presented which illustrates the sensitivity of a propeller to the flow field in which it is operating.

B. W. McCormick

THE AERODYNAMIC AND DYNAMIC BEHAVIOR of propellers for general aviation aircraft are of importance to the operation of these aircraft. A propeller which is poorly matched to its flow field or engine can be inefficient and subject to excessive vibratory stresses. The study of propeller aerodynamics and dynamics described here is divided into three parts. The first part deals with predicting the flow field in which the propeller is to operate. Here, a numerical method is described for calculating the velocity vector at any radial and azimuthal location in the propeller plane as a function of wing-fuselage-nacelle geometry. The second part treats both the steady and unsteady airloads produced by the propeller blades moving through the spatially varying velocity field. The third, and final section, examines the structural dynamics of the blades and presents methods for predicting their normal modes. In essence this paper is a brief summary of references 1, 2, and 3. For more details, a study of these references is recommended.

PROGRAM FOR PREDICTION OF PROPELLER FLOW FIELD

Potential flow methods, at least for tractor propellers, will accurately predict the velocity field in which a propeller operates since the effect of viscosity ahead of a body is usually negligible. However, even with the simplifications afforded by potential flow, the calculations for a fuselage-wing combination can prove tedious. Therefore, part of this study investigated the accuracy with which one needs to model the complete aircraft geometry in order to obtain a sufficiently precise velocity field at the propeller plane.

NUMERICAL MODEL

Hess

Following the lead of references 4 and 5, the fuselage surface is divided into a number of small panels as illustrated in a general sense in figure 1. Each panel is covered with a constant distributed source strength per unit area denoted by $\sigma(I)$. The velocity induced by the I^{th} panel on the surface of that panel directed outward and normal to the panel at the control point will be given by

Woodward

B. W. McCormick

$$V_N = \frac{\sigma(I)}{2} \qquad (1)$$

For any other panel, say the J^{th} panel, the total source strength over the panel is given by

$$Q(J) = \sigma(J)\ S(J) \qquad (2)$$

In order to calculate the velocity induced at the I^{th} panel by Q(J), Q(J) is taken to be a point source located on the J^{th} panel control point. Letting $\phi(J)$ denote the velocity potential associated with Q(J) and $\bar{N}(I)$, the unit vector normal to the I^{th} panel and directed outward, the velocity induced by Q(J) normally outward at the I^{th} panel will be

$$V_N(I,J) = \text{grad}\ \phi(J) \cdot \bar{N}(I) \qquad (3)$$

If $\bar{V}$ is the free-stream velocity vector and $\bar{V}_w(I)$ is the wing induced velocity vector at the I^{th} panel, the components of these vectors normally outward at the I^{th} panel control point will be

$$\bar{V} \cdot \bar{N}(I)$$

and,

$$\bar{V}_w(I) \cdot \bar{N}(I)$$

The normal velocity must vanish at panel I if it is a solid boundary or must equal the specified through velocity, q, normal across the panel if it is a relaxed boundary which models a region of through flow. Satisfying the appropriate boundary condition on panel I, it follows that

$$\bar{V} \cdot \bar{N}(I) + \bar{V}_w(I) \cdot \bar{N}(I) + \frac{\sigma(I)}{2} + \sum_{J=1}^{N} V_N(I,J)$$

$$= \begin{cases} 0 \text{ (solid boundary)} \\ q \text{ (relaxed boundary)} \end{cases} (J \neq I) \qquad (4)$$

For a point source of strength Q, the velocity potential ia given by,

$$\phi = -\frac{Q}{4\pi r} \qquad (5)$$

B. W. McCormick

where r is the radial distance from the source.

Writing,

$$\bar{V} = \bar{i}u + \bar{j}v + \bar{k}w \qquad \text{(a)}$$

$$\bar{V}_w(I) = \bar{i}u_w(I) + \bar{j}v_w(I) + \bar{k}w_w(I) \qquad \text{(b)} \quad (6)$$

$$\bar{N}(I) = \bar{i}n_x(I) + \bar{k}n_y(I) + \bar{k}n_z(I) \qquad \text{(c)}$$

Equation 4 can be written as,

$$\begin{aligned}
&[u + u_w(I)]n_x(I) + [v + v_w(I)]n_y(I) \\
&\quad + [w + w_w(I)]n_z(I) + \frac{\sigma(I)}{2} \qquad (7) \\
&\quad + \frac{1}{4\pi} \sum_{J=1}^{N} \frac{\sigma(J)\ S(J)}{R^3(I,J)} \{[x(I) - x(J)]n_x(I) \\
&\quad + [y(I) - y(J)]n_y(I) + [z(I) \\
&\quad - z(J)]n_z(I)\} = \begin{cases} 0 & \text{(solid boundary)} \\ q & \text{(relaxed boundary)} \end{cases} \\
&\qquad (J \neq I)
\end{aligned}$$

where,

$$R(I,J) = \{[x(I) - x(J)]^2 + [y(I) - y(J)]^2 + [z(I) - z(J)]^2\}^{\frac{1}{2}}$$

Letting I = 1, 2, ..., N, the foregoing represents a set of N simultaneous equations for the unknowns $\sigma(I)$. In order to solve this set of equations, the surface of a given body is divided into N panels that can be either four-sided or triangular. The task of paneling is a formidable one requiring care in the indexing of the corners. In the case of the non-planar, four-sided panel, the unit normal is obtained from the vector product of the diagonals. The panel area is then taken as the area of the panel projected on a plane perpendicular to this unit vector. Arithmetic averages of the x, y, and z positions of the four corners define the location of the control point and concentrated source for this type of panel. Control points and concentrated sources are located at the centroid of triangular panels.

Once the $\sigma(I)$ values are obtained, the velocity field at any point can be determined by combining the free stream velocity and local wing induced velocity vectors with the gradient of ϕ obtained from equations 2 and 5. The total ϕ, of course, is obtained by summing over the index I. The complete program which has been developed will handle both wing-fuselage and wing-fuselage-nacelle combinations as shown in figure 2. By employing the relaxed boundary condition in equation 7 on particular panels, it also allows for flow through a panel to represent air intakes or exhausts. The lifting wing is modeled simply by a single horseshoe vortex placed along the quarter-chord line (unswept) and trailing from the $\pi/4$ spanwise station. This simple model is considerably easier to handle computationally compared to vortex lattice models and results in upwash velocities at typical propeller locations that are within a few percent of more exact calculations. As equation 7 indicates, the effect of the vortex on the body is considered in determining the $\sigma(I)$ values. However, the effect of the fuselage or nacelles on the wing is not taken into account.

The final program has been checked against closed-form solutions and the results compare favorably, at least for simple, nonlifting body shapes. It was then applied to typical fuselage shapes with a certain amount confidence. These results will be described later.

METHOD FOR PREDICTING AERODYNAMIC LOADS ON A PROPELLER

A propeller operating at an angle of attack or in the presence of a fuselage experiences time-dependent aerodynamic loads as its blades pass through a spatially varying velocity field. Generally, both the magnitude and direction of the velocity field will be a function of blade position. Thus blade section lift coefficients and resultant velocities vary periodically with the blade azimuth angle.

In order to predict the unsteady forces on a propeller blade, it is convenient to consider first the steady case. A section of a propeller blade as viewed looking toward the hub along the blade is pictured in figure 3. The blade section is operating under the influence of three velocity components: the free stream velocity, V; the linear velocity due to rotation, ωr; and the induced velocity, w. The modern trend is to calculate the induced velocity w by applying the Biot-Savart relationship to the propeller's helical trailing vortex system. Even here, however, it is usually necessary to assume a shape to the wake before numerically integrating the Biot-Savart equations. A free-wake analysis, where the location of the trailing vortex system and its induced velocities are mutually dependent, requires a prohibitive amount of computer time.

A propeller application of classical vortex theory incorporating corrections for profile drag, finite section thickness, and finite chord appears to predict propeller thrust and torque in close agreement with experimental measurements over a wide range of propeller geometries. This method, used here, is much simpler to apply by comparison to vortex lattice methods. The details can be found in references 1, 6, and 7 and will not be repeated here. However, a few points will be noted.

1. An accurate empirical correlation of section C_d with α and Mach number for Clark-Y, series 16 and NACA 4-digit airfoil sections is to be found in reference 1.

2. The tangential component of w is related to the bound circulation through Prandtl's tip loss factor F. Reference 1 shows that this closed form approximation to Goldstein's kappa factor gives predicted results very close to those obtained using kappa.

3. Normality between w and the resultant velocity is assumed in the propeller plane. This assumption is justified in reference 7.

4. The tip angle of the helical vortex wake necessary to the calculation of F is obtained by iterating on w. Figures 4 and 5 are two typical results of steady propeller performance predictions to be found in reference 1. The agreement shown in figure 5 between predictions and experimental results is particularly impressive considering the fact that the resultant tip Mach number exceeds 1.0 for advance ratios greater than 1.2.

CALCULATION OF UNSTEADY PROPELLER AERODYNAMIC LOADS

The prediction of unsteady aerodynamic loads builds on the steady case. Generally, under the influence of angle of attack, wing upwash, and body interference, the propeller operates in a velocity field which varies both radially and circumferentially. The approach taken here is to express the axial and tangential velocity components relative to the propeller at a given radius as the sum of harmonics of ψ, the azimuth angle. ψ is defined in figure 6.

Let V_{AN} and V_{TN} denote the N^{th} harmonics of the axial and tangential velocity components respectively at a particular radius. That is,

$$V_{AN} = [a_{AN} \cos N\psi + b_{AN} \sin N\psi]V \quad \text{(a)}$$

$$V_{TN} = [a_{TN} \cos N\psi + b_{TN} \sin N\psi]V \quad \text{(b)} \qquad (8)$$

Combining V_{AN} and V_{TN} vectorially, the N^{th} harmonic or the velocity vector normal to the steady resultant velocity V_e, shown in figure 7, can be written as,

$$V_{NN} = V_{AN} \cos (\phi + \alpha_i) - N_{TN} \sin (\phi + \alpha_i) \qquad (9)$$

Combining equations 8 and 9 gives,

$$\begin{aligned} V_{NN}/V = {} & [a_{AN} \cos (\phi + \alpha_i) \\ & - a_{TN} \sin (\phi + \alpha_i)] \cos N\psi \qquad (10) \\ & + [b_{AN} \cos (\phi + \alpha_i) - b_{TN} \sin (\phi \\ & + \alpha_i)] \sin N\psi \end{aligned}$$

By comparison to an airfoil undergoing a pure heaving motion, V_{NN} corresponds to the heaving velocity $\dot{h}$. The heaving acceleration $\ddot{h}$ is given by differentiating V_{NN} with respect to time. Since $\omega = d\psi/dt$ it follows that,

$$\begin{aligned} \ddot{h}/V = {} & -N\omega[a_{AN} \cos (\phi + \alpha_i) \\ & - a_{TN} \sin (\phi + \alpha_i)] \sin N\psi \qquad (11) \\ & + N\omega[b_{AN} \cos (\phi + \alpha_i) \\ & - b_{TN} \sin (\phi + \alpha_i)] \cos N\psi \end{aligned}$$

Knowing $\dot{h}$ and $\ddot{h}$, one can calculate the unsteady lift on the heaving airfoil from

$$L = \frac{\pi \rho c^2}{4} h + \pi \rho V c C(k) \dot{h} \qquad (12)$$

The above can be found in reference 8. C(k) is a complex function known as Theordorsen's function while k is the so-called reduced frequency defined by,

$$k = \frac{\omega c}{2V} \qquad (13)$$

Here ω is the circular frequency of the harmonic heaving motion which in this case is equal to the rotational speed of the propeller. The complex function C(k) is frequently seen expressed as,

$$C(k) = F(k) + iG(k) \qquad (14)$$

C(k) is presented in figure 8.
Thus,

$$L/\dot{h} = \pi \rho V c F + i\left[\frac{\pi \rho c^2}{4} + \pi \rho V c G\right] \qquad (15)$$

This can be written in the dimensionless form,

$$\frac{L}{\pi \rho V c \dot{h}} = \sqrt{F^2 + \left(\frac{k}{2} + G\right)^2} \quad e^{i\phi} \qquad (16)$$

where:

$$\phi = \tan^{-1} \frac{\frac{k}{2} + G}{F}$$

Thus, equation 16 relates the amplitude and phase of the unsteady section left, L, to the heaving velocity $\dot{h}$. ϕ is the angle by which the lift force leads $\dot{h}$. Substituting V_{NN} (equation 10) for $\dot{h}$ thus leads to the amplitude and phase for the sectional unsteady lift on the propeller blade. This lift can be resolved into thrust and torque components and then integrated over the blade length to give the total unsteady forces and moments acting on the blade.

The computer program which accomplishes the foregoing is described in reference 1. As input this program requires the axial and tangential velocity components relative to the propeller axis and in its disk plane. These are obtained directly as output from the program developed in reference 3. These are then Fourier-analyzed by the former program to obtain the a_{AN}, A_{TN}, b_{AN}, and b_{TN} coefficients. Generally, the first harmonic is the predominant one. In the results to follow, only the first two harmonics are used although the program is capable of handling up to eight.

RESULTS OF UNSTEADY AIRLOAD CALCULATIONS

A propeller in a uniform flow inclined at an angle to the flow of α experiences only a first harmonic variation in its inflow. In this case, it is easily shown that,

$$a_{AN} = 0 \quad \text{(a)}$$

$$a_{TN} = 0 \quad \text{(b)}$$

$$b_{AN} = 0 \quad \text{(c)} \qquad (17)$$

$$b_{T1} = \sin\alpha \quad \text{(d)}$$

$$b_{TN} = 0 \quad \text{for } N > 1 \quad \text{(e)}$$

With this input, and first solving for the steady loads in order to get $(\phi + \alpha_i)$, the results presented in figures 9 and 10 were obtained. It should be noted that V cos α must be used as the steady inflow velocity for the propeller at an angle of attack.

Figure 9 presents the azimuthal variation of the gradient section of the thrust at the 0.75 station for a 3-bladed propeller at a 4.6° angle of attack. ΔC_T, the increment in the thrust coefficient due to the unsteadiness is defined in accordance with standard terminology as,

$$\Delta C_T = \frac{\Delta T}{\rho n^2 D^4} \qquad (18)$$

Three curves are shown on the graph. The experimental curve is taken from reference 9. The curve labeled "predicted, 2D unsteady" is based on the methods just described. In figure 10, the gradient of ΔC_T with respect to the dimensionless radius, x, is presented. The quasi-steady calculations were performed by simply assuming that steady aerodynamics could be applied to the instantaneous section velocity diagram. This is tantamount to using a C(k) value of unity in equation 12 and neglecting the $\ddot{h}$ term in that equation.

The simpler, quasi-steady approach results in predictions which are close to experimental results in amplitude but are shifted somewhat in phase. The unsteady 2D aerodynamic calculations generally have the correct phase but tend to overpredict the amplitudes of the unsteady forces. As shown, the amplitude of unsteady thrust is appreciable for this case, being of the order of 25% of the steady loading.

Now consider the case of a propeller operating on a typical single-engine, light airplane, in this case, a Piper Cherokee 180. The Department of Aerospace Engineering at The Pennsylvania State University owns and operates this particular airplane; hence its choice. To begin, the cowling of the Cherokee was carefully measured using surveying transits in order to define its contour. Aft of the cowling, 3-view drawings were assumed to be adequate. Using this fuselage geometry, calculations of the velocity field at the propeller plane were performed for two different fuselage angles of attack of 8° and 2°. The higher angle corresponds to an airspeed of approximately 35.8 m/s (80 mph) while the lower angle is typical of cruising conditions of approximately 55.0 m/s (123 mph). Calculated tangential and axial velocity distributions at the propeller plane are presented in figure 11 for the 2° angle of attack case. Figures 12 and 13 present the first two harmonic amplitudes for both 2° and 8° as a function of propeller radius. Not unexpectedly, the amplitudes are seen to increase toward the hub. Also, observe that the axial component of velocity is not as dependent on α as the tangential component. The slight asymmetries about ψ values of 0° and 180° shown in figure 11 result from the fact that these components are relative to the propeller plane which is yawed slightly with respect to the fuselage plane of symmetry.

The calculation of the axial and tangential velocities in the plane of the propeller depend primarily on the shape of the cowling and angle of attack. The latter results directly in a tangential component and also determines the upwash generated by the wing. The insensitivity of the flow field to the fuselage geometry aft of the cowling is shown in figure 14. In one case the complete fuselage is modeled. In the other, the fuselage is cut off behind the cowling and replaced by a smaller afterbody which can be defined using fewer panels. This simplification saves computation time and is seen to have almost no effect on the velocity field except near the top where $\psi = 0$ and the elimination of the windshield has the greatest influence. Even here, however, the change in the velocity is only approximately 2%.

Using drawings of the propeller for the Cherokee 180 propeller supplied by the manufacturer and the calculated velocity field, predictions have been made of the propellers steady and unsteady performance. Figure 15 presents the predicted steady performance of the Sensenich propeller used on the Cherokee 180. Series 16 airfoil sections were assumed in making these predictions since their contours can be closely matched to the special sections developed and used by Sensenich. These results are typical of those to be found in the NACA reports such as reference 10. The propeller appears to be well matched to the airplane in the cruise condition where it operates at an advance ratio of 0.75.

Figure 16 illustrates the unsteady results which were obtained for the Cherokee 180. Here, the first harmonic of the unsteady thrust gradient for angles of attack of 2° and 8° is presented as a function of the radial position along the blade. Note that the predicted amplitude of the unsteady thrust is nearly constant along the blade. The steady loads, of course, increase toward the tip but this is not so, at least in this example, for the unsteady loads. The unsteady velocity components apparently decrease with increasing radius so as to compensate for the increasing resultant velocities due to ωr.

PROPELLER BLADE DYNAMICS

The unsteady aerodynamic forces just discussed will excite a dynamic response from the propeller blades. Added to this excitation will be, of course, any unsteady torque impulse from the engine crankshaft. In order to predict fatigue stresses on the propeller blades, one must in the final analysis treat the complete engine-propeller dynamic system. As an important part of the complete analysis, a study has been undertaken of the structural dynamic behavior of the propeller as an isolated body. The object of this study, which has been accomplished, was to develop a method for predicting the normal modes of vibration for a propeller for the case where the hub is rigidly clamped. These modes are determined experimentally by propeller manufacturers to assure that none of the lower modes coincide with the exciting frequencies from the powerplant. However, the testing is normally performed with the propeller supported as a free body.

It was hoped to model coupled in plane bending-out of plane bending torsion motion. While this goal has proven to be elusive, a computer program has been developed which will predict the normal modes for coupled bending-bending or bending-torsion motion. Since propeller blades are very stiff in plane and torsionally the lower modes of the coupled bending-bending and coupled bending-torsion modes have approximately the same frequencies which are determined principally by the relatively soft flapwise (out of plane) bending stiffness. Thus failure to model the coupled bending-bending-torsion motion is not considered to be too serious.

A major accomplishment of this study has been the development of a program to calculate the shear center location for a solid cross-section having an airfoil-like shape. This program, based on a membrane analogy, and soap film theory, will accept as input discrete points on an airfoil contour or an analytical definition of the contour. Some results of this program are presented in figure 17. Within a given airfoil family, the position of the shear center is seen to be nearly constant. However, the chordwise position differs significantly between the NACA 4-digit and series 16 airfoil families. In addition to the location of the shear center, this program also calculates the location of the section center of gravity, principal axes and moments of inertia. All of these section properties are required in order to calculate the normal mode shapes and frequencies. These section properties for the Sensenich propeller model 76EM8-0-61 are presented in figure 18.

The relationships on which the computer program for determining the normal modes are based are too lengthy to be presented here. They can be found in reference 3 and depend on the concept of a transmission matrix. The original source for much of this analysis can be found in reference 11.

The predictions of natural frequencies have been confirmed by comparison to measurements provided by the manufacturer and by our own testing. The experimental setup which was used is shown schematically in figure 19. The propeller was excited as a free body by placing it on a soft bed made from two innertubes. In order to cantilever a blade, the hub was clamped in a Universal Testing machine. Even though the mass of the machine is large and the clamping pressure high it was necessary to weight the blade opposite the one being excited in order to avoid spurious modes.

Some of the experimental and calculated results for the Sensenich propeller are shown in Table 1. Generally, the frequencies which were obtained experimentally for the first four symmetric modes of the propeller supported freely confirm those found by the manufacturer. With the hub clamped, the predicted frequencies for the first modes for coupled bending-bending and coupled bending-torsion are nearly equal and close to the frequency measured for the cantilevered blade.

The predicted mode shapes for the first three modes for the clamped propeller are presented in figure 20. The predicted frequencies for these modes are given in figure 21 as a function of propeller rotational speed. Also included in this figure are the results supplied by Sensenich for the freely-supported propeller. Centrifugal stiffening is seen to increase the natural frequencies of each mode slightly as the propeller speed increases. Superimposed on this figure are lines representing integer multiples of the torque impulse from the engine. Since half of the cylinders of a four-cycle, horizontally-opposed engine fire during each revolution, the fundamental impulse frequency for the four cylinder Cherokee 180 engine in cycles per second, is

$$F = \left[\frac{\text{no. of cylinders}}{2} \right] \left(\frac{\text{rpm}}{60} \right) \text{ Hz}$$

$$F = \left[\frac{\text{rpm}}{60} \right] \text{ Hz}$$

This type of diagram, where exciting frequencies are superimposed over natural frequencies is frequently applied to rotating systems other than propellers and is known as a Southwell diagram. In order to avoid excessive vibration, the operational rotational speed of the system, in this case the propeller rpm, should be selected so that none of the natural frequencies and exciting frequencies are coincident. In the case of the Cherokee 180, the recommended cruising rpm of 2500 is above both the first and second modes of either the cantilevered or freely-supported blade.

SUMMARY

A study of the aerodynamics and dynamics of propellers for general aviation aircraft has resulted in the development of three computer programs. The analytical bases for these programs can be found in references 1, 2, and 3. In addition, user's manuals are currently being prepared together with program listings in FORTRAN. Briefly these programs

- calculate the velocity field in the propeller plane for a wing-fuselage-nacelle combination,
- predict the steady and unsteady propeller aerodynamic loads,
- predict the natural mode shapes and frequencies for the propeller up to the first four modes.

In the future, it is hoped to combine the programs in order to predict the forces exciting airframe vibration. A normal modes approach will probably be tried to accomplish this challenging task. In addition, it is also planned to obtain additional experimental confirmation of the existing programs.

REFERENCES

1. A. S. Aljabri, "Prediction of Propeller Performance and Loading in Uniform and Nonuniform Flowfields," M.S. Thesis, The Pennsylvania State University, November 1978.

2. Z. N. Martinovic, "A Study of the Dynamic Behavior of Propeller Blades," M.S. Thesis, The Pennsylvania State University, March 1979.

3. S. J. Jumper, "Computer Prediction of Three-Dimensional Potential Flowfields in which Aircraft Propellers Operate," M.S. Thesis, The Pennsylvania State University, March 1979.

4. J. L. Hess and A. M. O. Smith, "Calculation of Potential Flow About Arbitrary Bodies," Progress in Aeronautical Sciences, Pergammon Press, Vol. 8, 1967.

5. F. A. Woodward, F. A. Dvorak and E. W. Geller, "A Computer Program for Three-Dimensional Lifting Bodies in Subsonic Inviscid Flow," Report USAAMRDL-TR-74-18, April 1974.

6. D. V. Pauling, "The Effects of Uncertainties on Predicting Rotor and Propeller Performance," M.S. Thesis, The Pennsylvania State University, May 1975.

7. B. W. McCormick, Jr., "Aerodynamics of V/STOL Flight," Academic Press, New York, 1967.

8. R. L. Bisplinghoff, H. Ashley and R. L. Halfman, "Aeroelasticity," Addison-Wesley, 1955.

9. W. H. Gray, J. M. Hallissy, Jr. and A. R. Heath, Jr., "A Wind-Tunnel Investigation of the Effects of Thrust-Axis Inclination on Propeller First-Order Vibration," NACA TR 1205, 1954.

10. E. P. Hartman and D. Biermann, "The Aerodynamic Characteristics of Full-Scale Propellers Having 2, 3 and 4 Blades of Clark Y and R.A.F. 6 Airfoil Sections," NACA TR 640.

11. V. R. Murthy, "Dynamic Characteristics of Rotor Blades," Journal of Sound and Vibration, 49(4), pp. 483-500, 1976.

Table 1

NATURAL FREQUENCIES OF A NON-ROTATING SENSENICH PROPELLER

ω(Hz)

Mode Number	Free Beam Symmetric Modes		Cantilever Beam		
			Predicted Values		Experimental Data
	Sensenich Data	Experimental Data	Coupled Bending-Bending	Coupled Bending-Torsional	
1	56.8	58.2	51.7	51.4	50.0
2	170.0	175.0	161.5	168.1	139.0
3	342.9	347.0	312.7	372.3	316.0
4	486.6	431.0	384.8	664.0	434.0

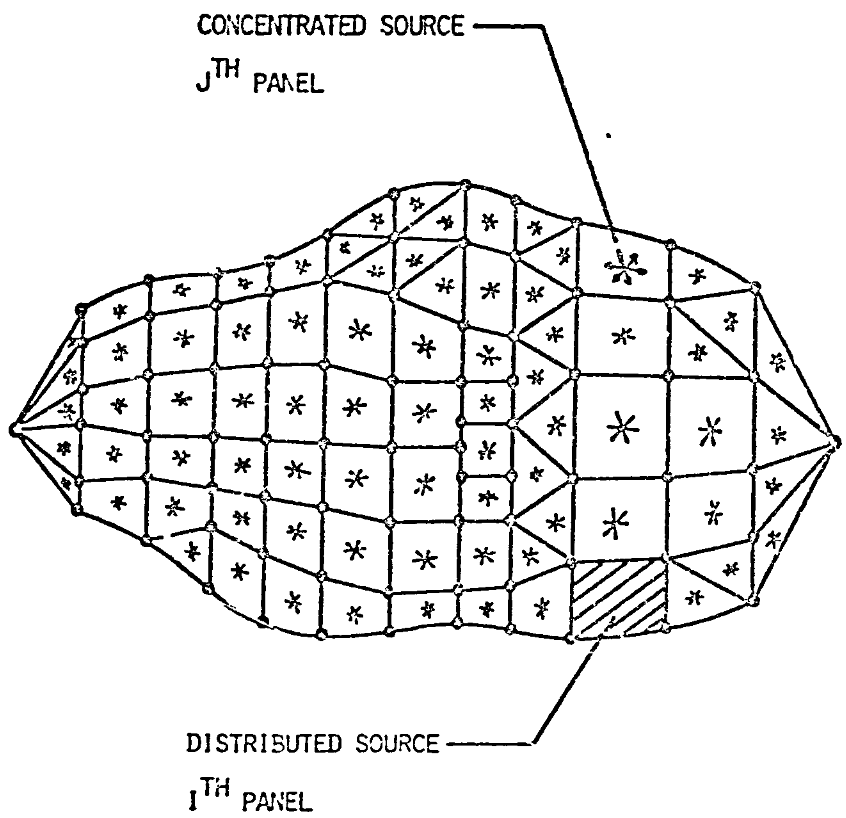

FIG. 1 PANELING OF BODY SURFACE

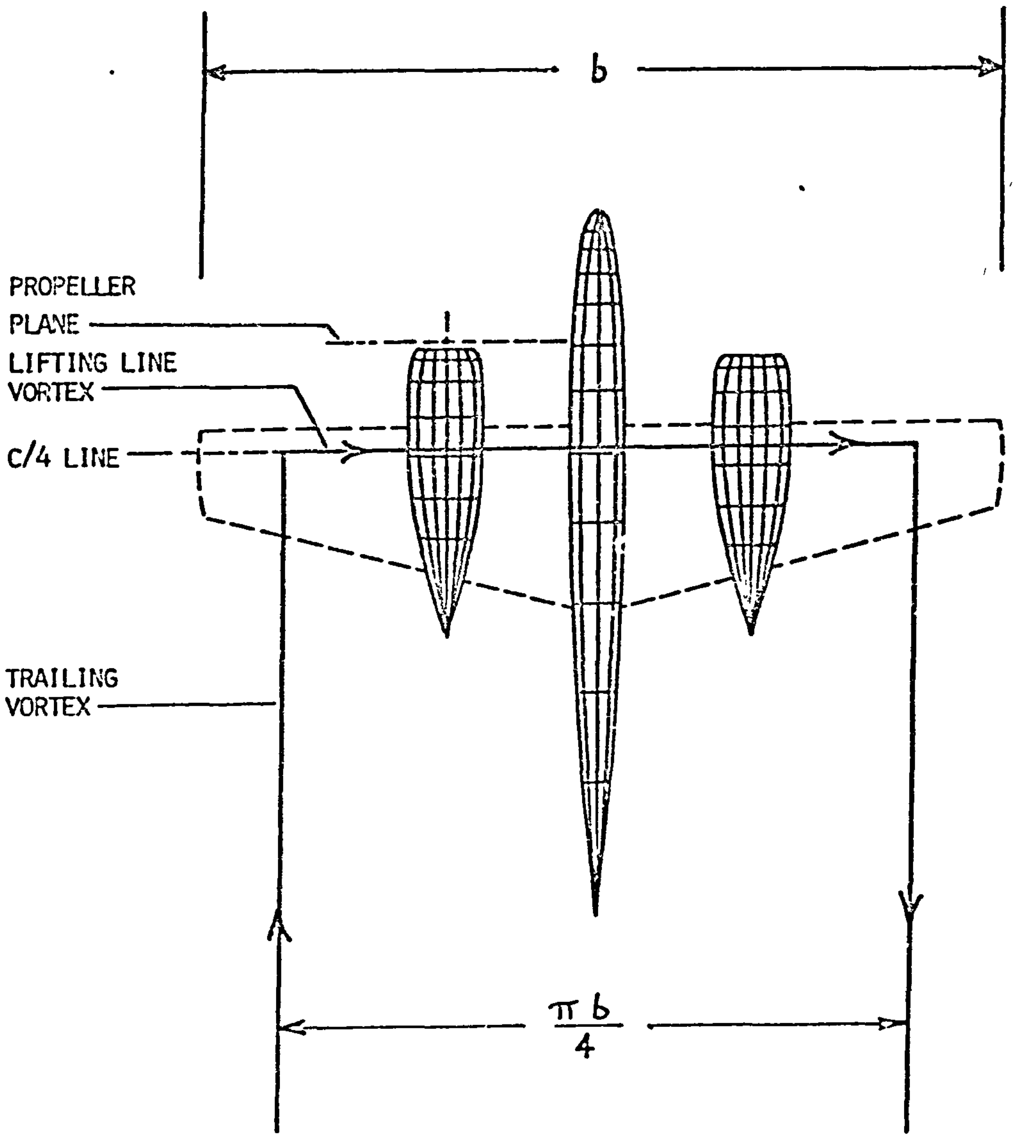

FIG. 2 SIMPLIFIED WING-FUSELAGE-NACELLE MODEL

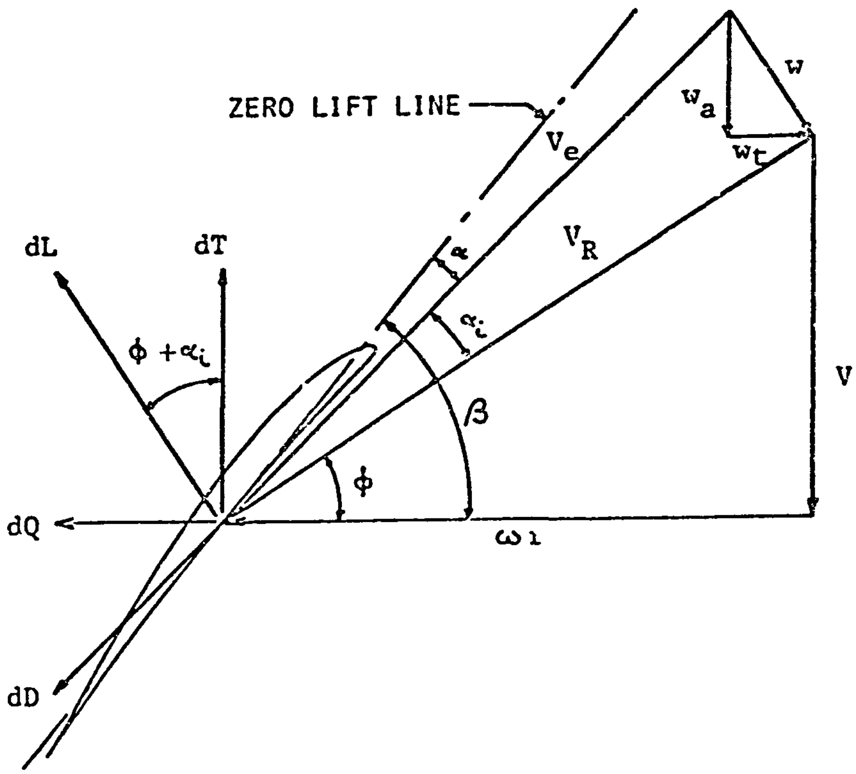

FIG. 3 VELOCITY DIAGRAM FOR BLADE SECTION

PROPELLER NACA 5868-9
CLARK Y SECTION
NO OF BLADES = 2,3 & 4.
BLADE ANGLE AT 3/4 STATION = 35°
ACTIVITY FACTOR = 78.9

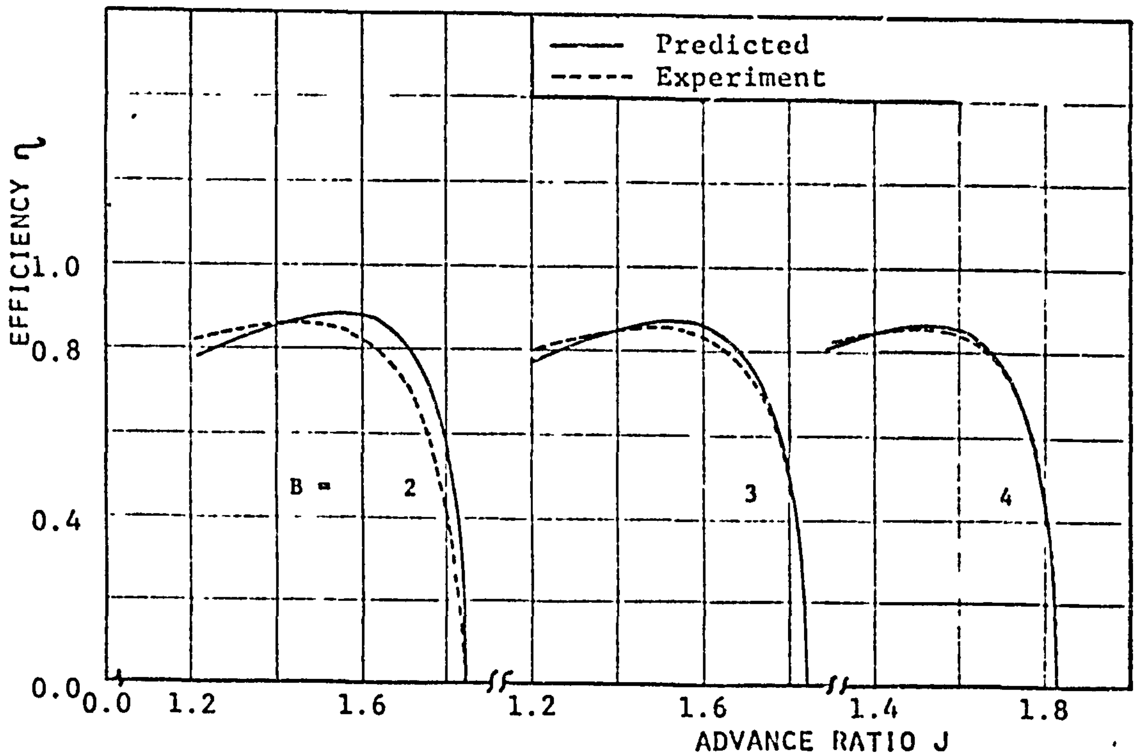

FIG. 4 COMPARISON OF PREDICTED AND MEASURED PROPELLER EFFICIENCY FOR DIFFERENT NUMBER OF BLADES

PROPELLER NACA 10-(3)(05)-045
NACA 16-SERIES SECTION
NO OF BLADES = 2
BLADE ANGLE AT 3/4 STATION = 20°, 25° & 35°
ACTIVITY FACTOR = 131.5
ROTATIONAL SPEED = 2000 RPM

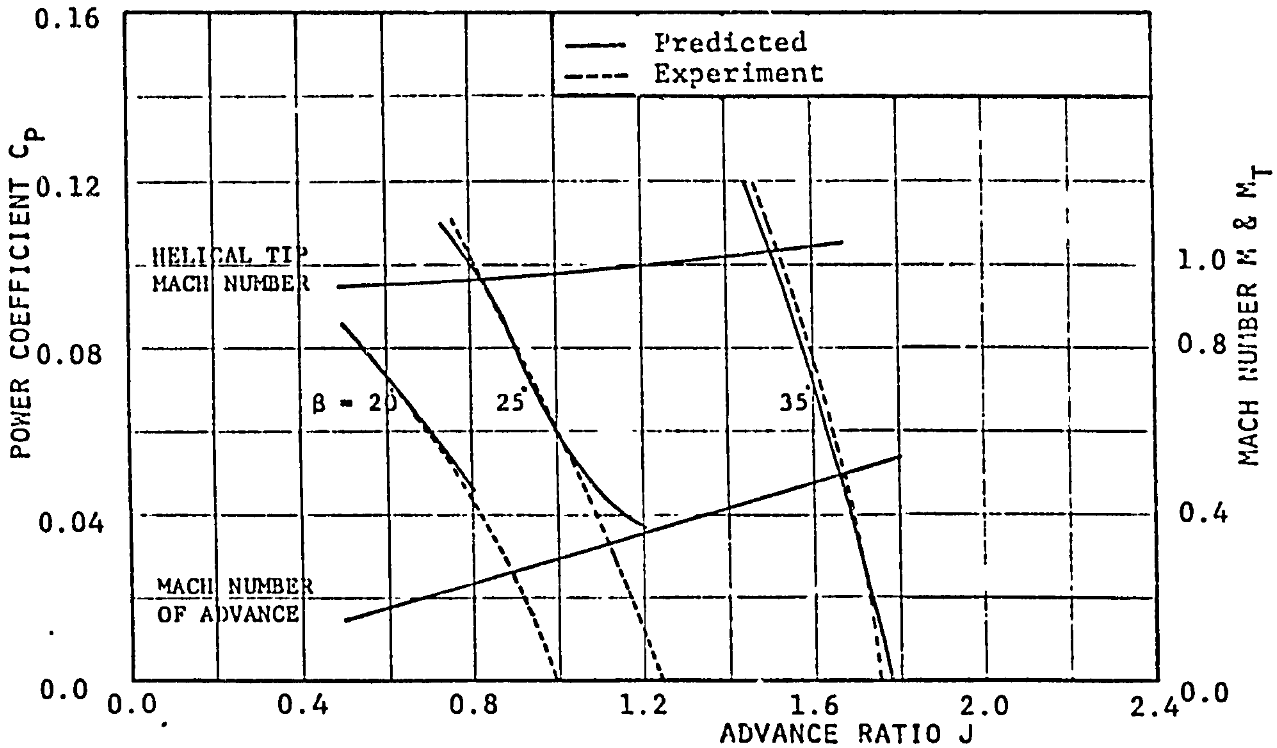

FIG. 5 COMPARISON OF PREDICTED AND MEASURED POWER COEFFICIENT AT 2000 R.P.M.

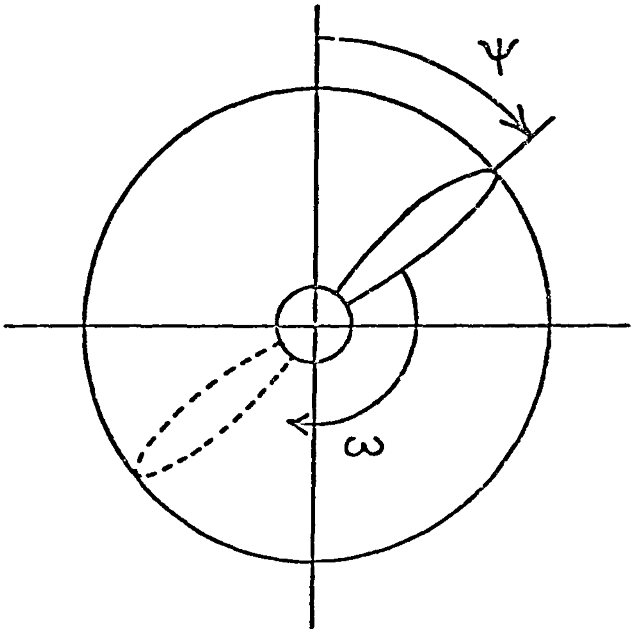

FIG. 6 VIEW OF PROPELLER LOOKING
IN DIRECTION OF FLIGHT

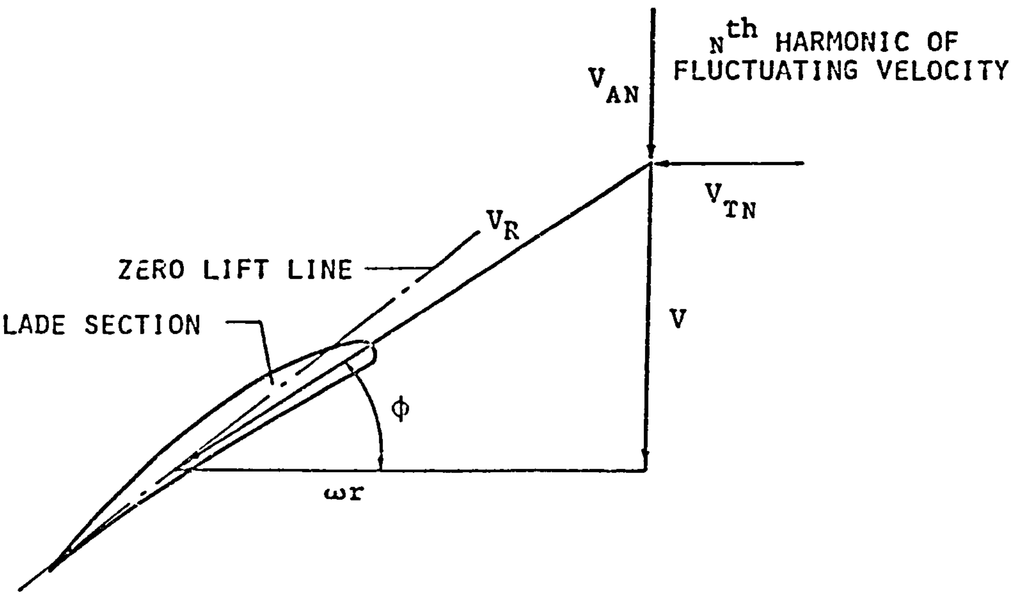

FIG. 7 N^{th} HARMONIC OF INFLOW VELOCITY FOR BLADE SECTION

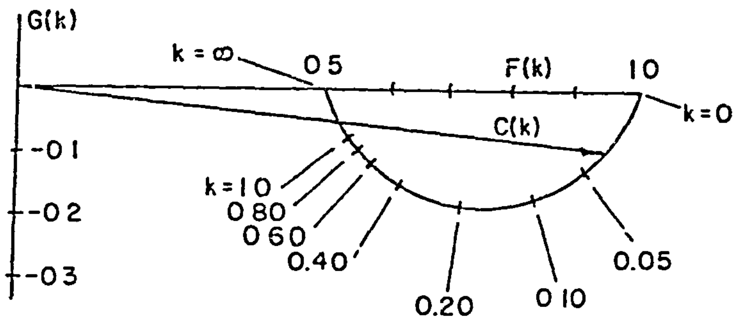

FIG. 8 THEORDORSEN'S FUNCTION

PROPELLER NACA 10-(3)(08)-03
NACA 16-SERIES SECTION
NO OF BLADES = 3
BLADE ANGLE AT 3/4 STATION = 30°
ACTIVITY FACTOR = 86.2
PROPELLER ANGLE OF ATTACK = 4.55°
ROTATIONAL SPEED = 1350 RPM
ADVANCE RATIO = 1.2

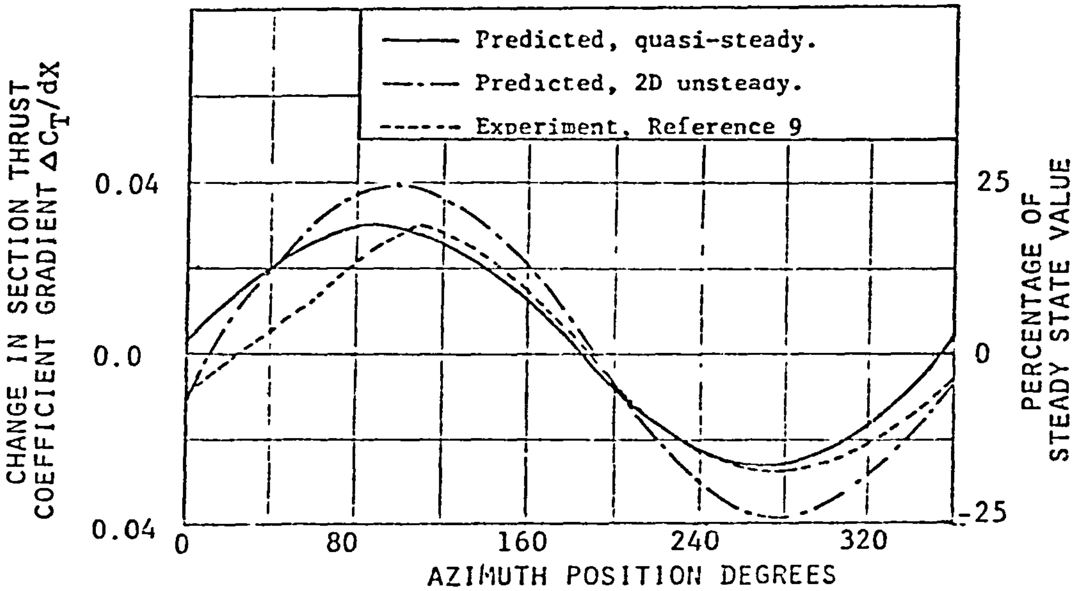

FIG. 9 CHANGE IN BLADE SECTION THRUST COEFFICIENT GRADIENT WITH AZIMUTHAL POSITION OF BLADE AT THE 3/4 RADIAL STATION

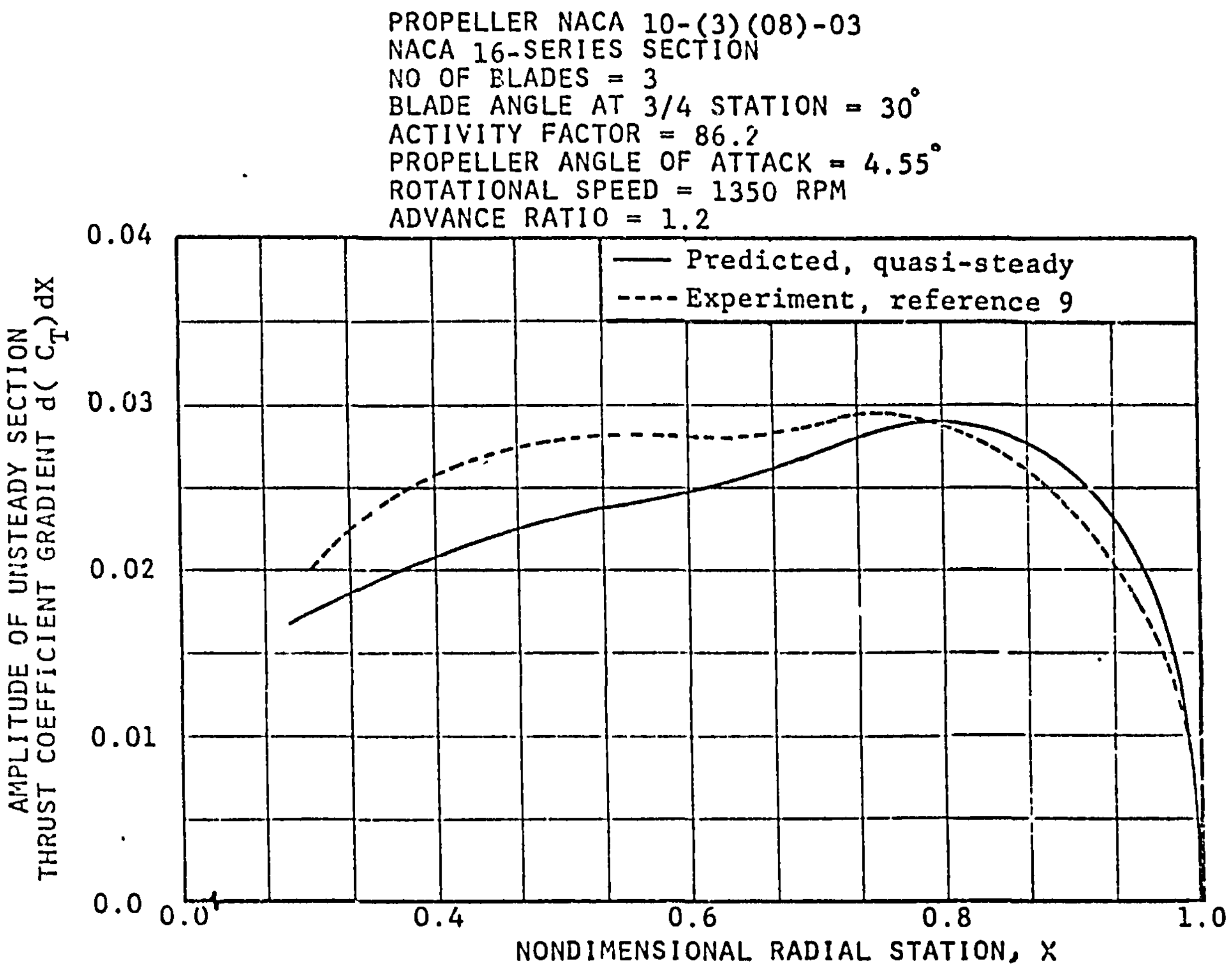

FIG. 10 DISTRIBUTION OF AMPLITUDE OF UNSTEADY SECTION THRUST COEFFICIENT GRADIENT

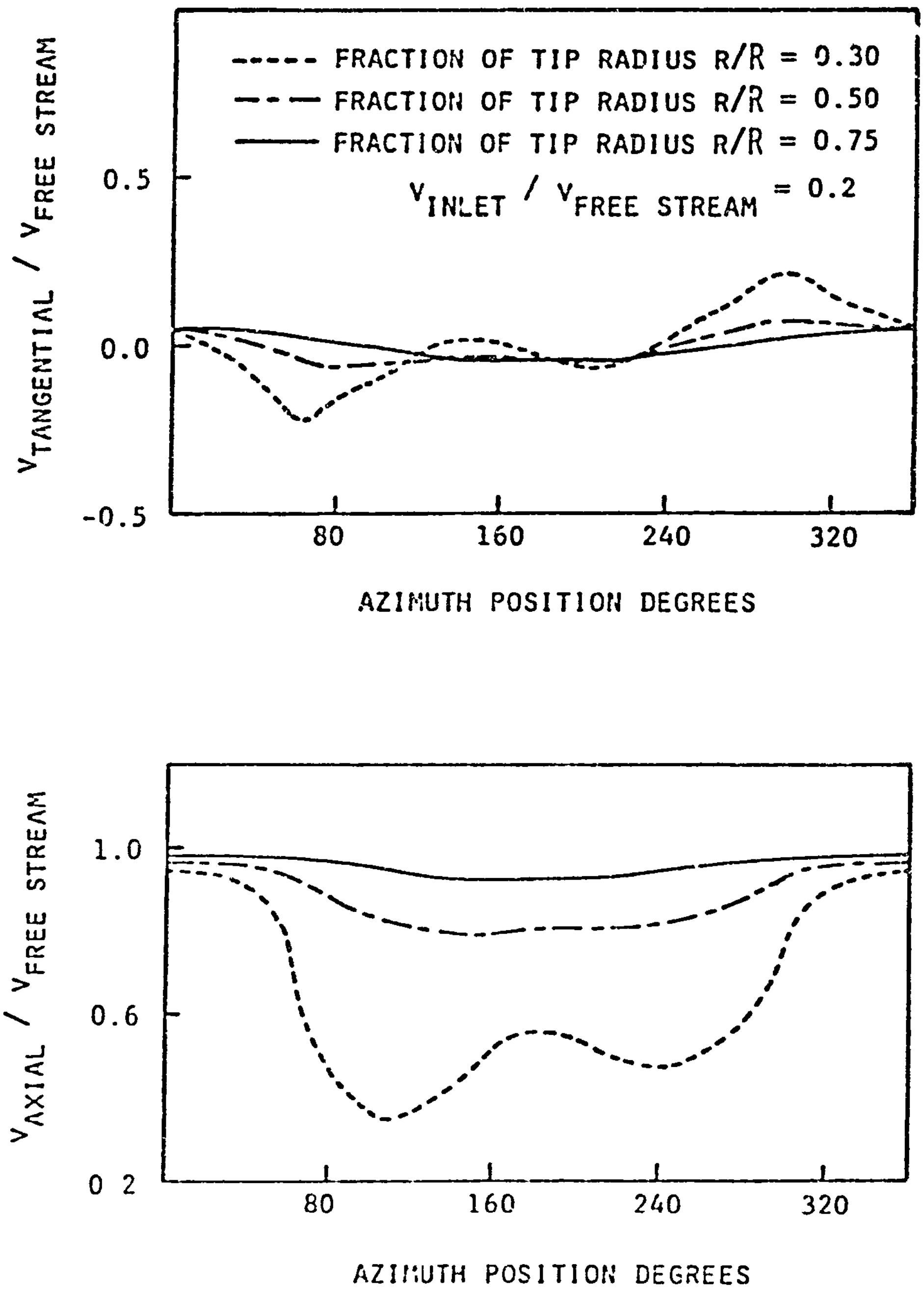

FIG. 11 PREDICTED AZIMUTHAL DISTRIBUTION OF AXIAL AND TANGENTIAL VELOCITIES IN THE PROPELLER PLANE OF A PIPER CHEROKEE 180. FUSELAGE ANGLE OF ATTACK = 2.0°, C_L = .385

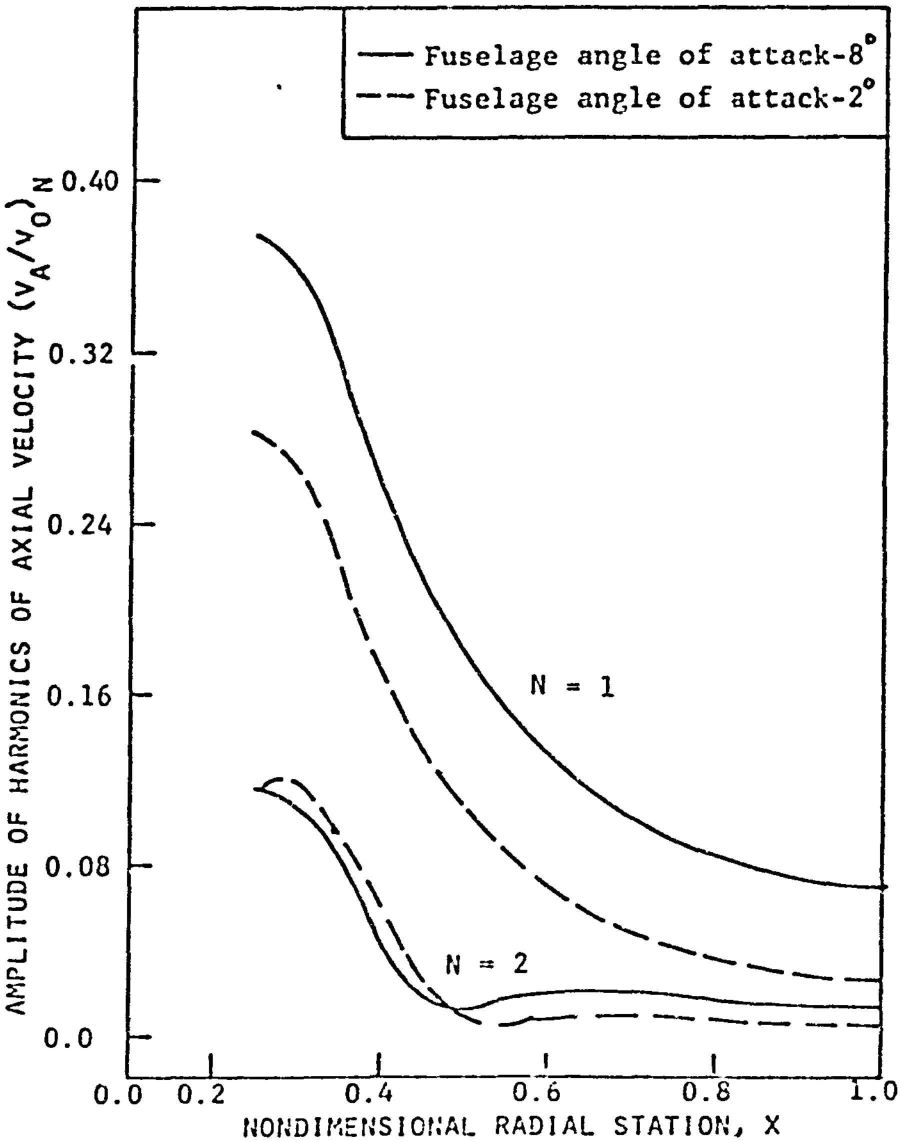

FIG. 12 HARMONIC CONTENT OF THE AXIAL VELOCITY DISTRIBUTION IN THE PROPELLER PLANE OPERATING IN THE FLOW FIELD OF A PIPER CHEROKEE 180

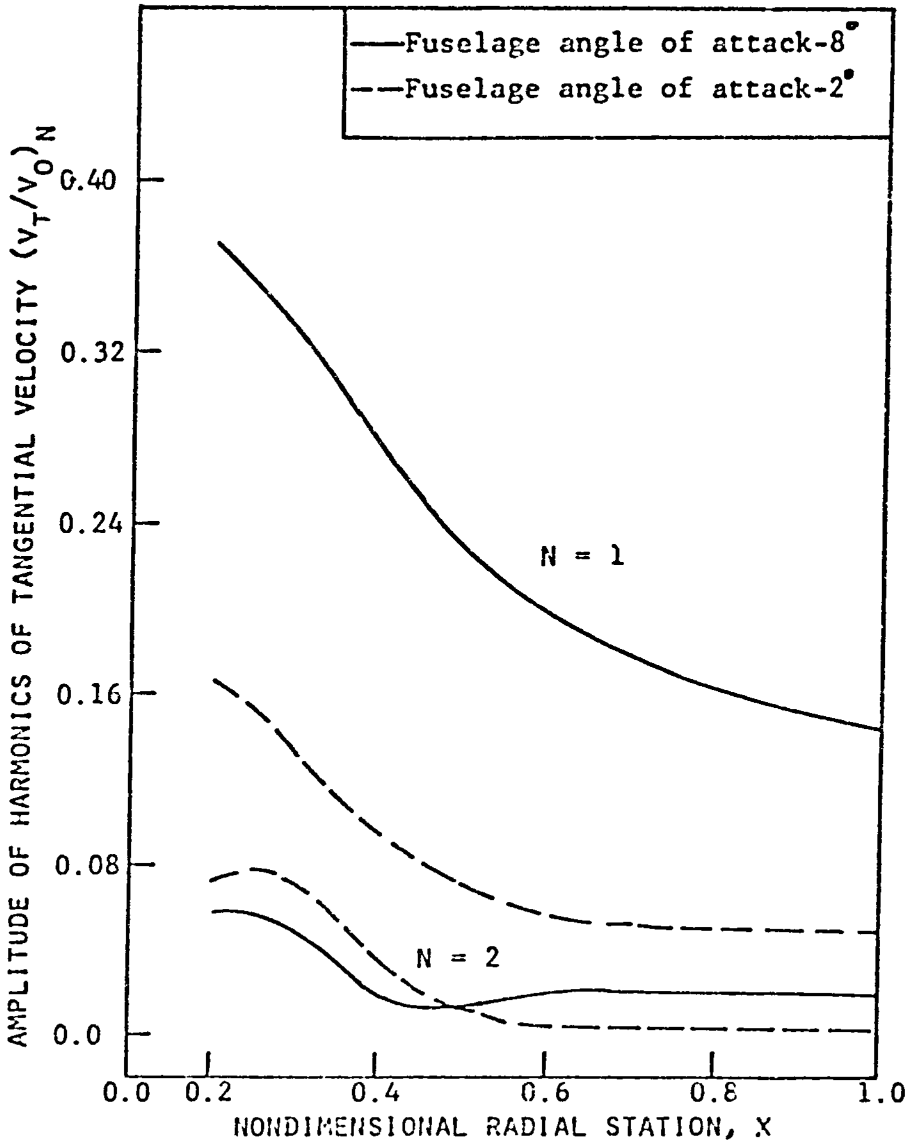

FIG. 13 HARMONIC CONTENT OF THE TANGENTIAL VELOCITY DISTRIBUTION IN THE PROPELLER PLANE OPERATING IN THE FLOW FIELD OF A PIPER CHEROKEE 180

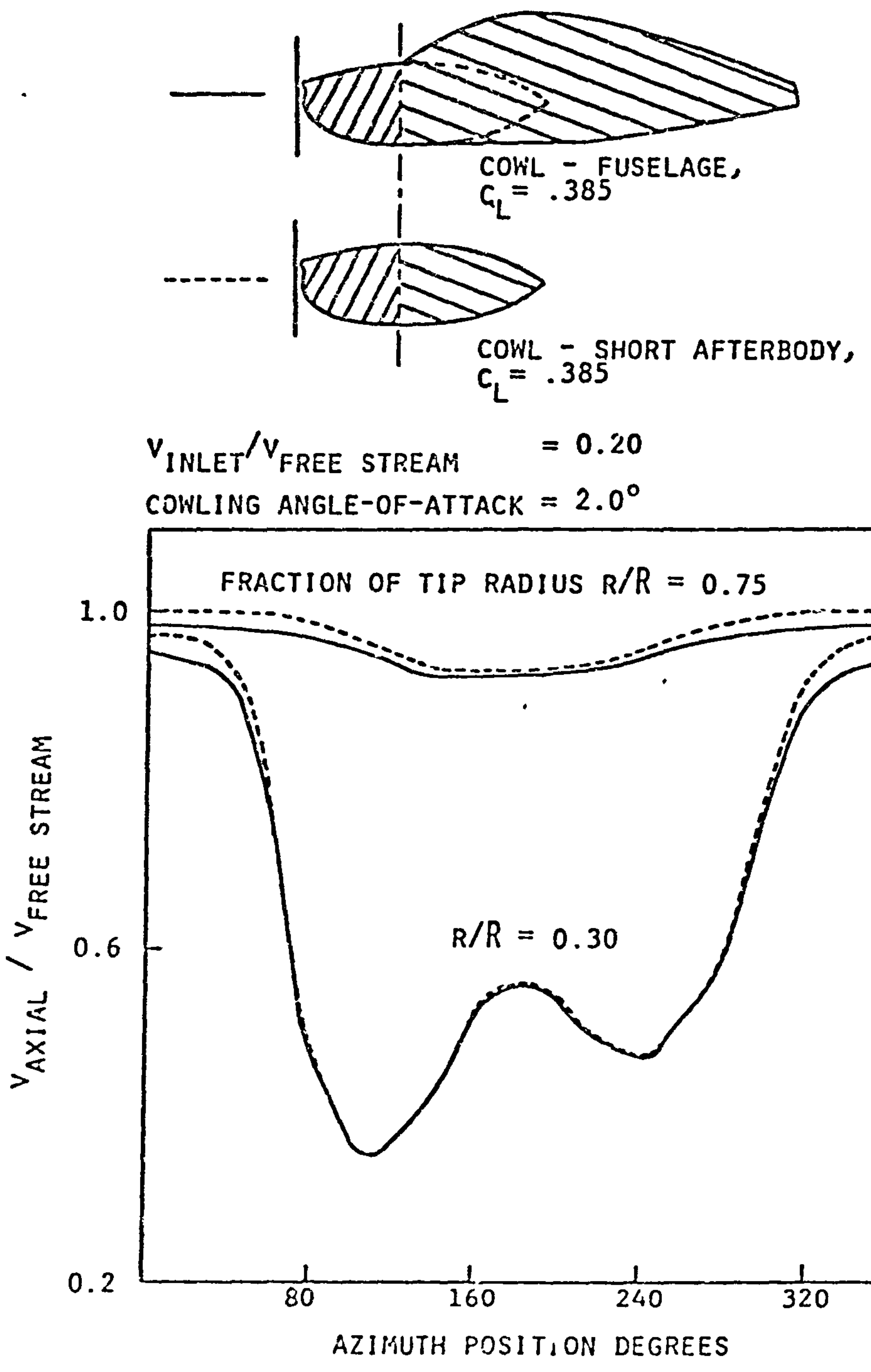

FIG. 14 COMPARISON OF AZIMUTHAL DISTRIBUTIONS OF AXIAL VELOCITY IN THE PROPELLER PLANE OF A PIPER CHEROKEE 180 PREDICTED USING TWO DIFFERENT BODY GEOMETRY MODELS AFT OF THE COWLING

PROPELLER SENSENICH 76EM8-0-61
EQUIVALENT NACA 16-SERIES SECTION
NO OF BLADES = 2
BLADE ANGLE AT 3/4 STATION = 18.5
ACTIVITY FACTOR = 94.4
ROTATIONAL SPEED   2700 RPM

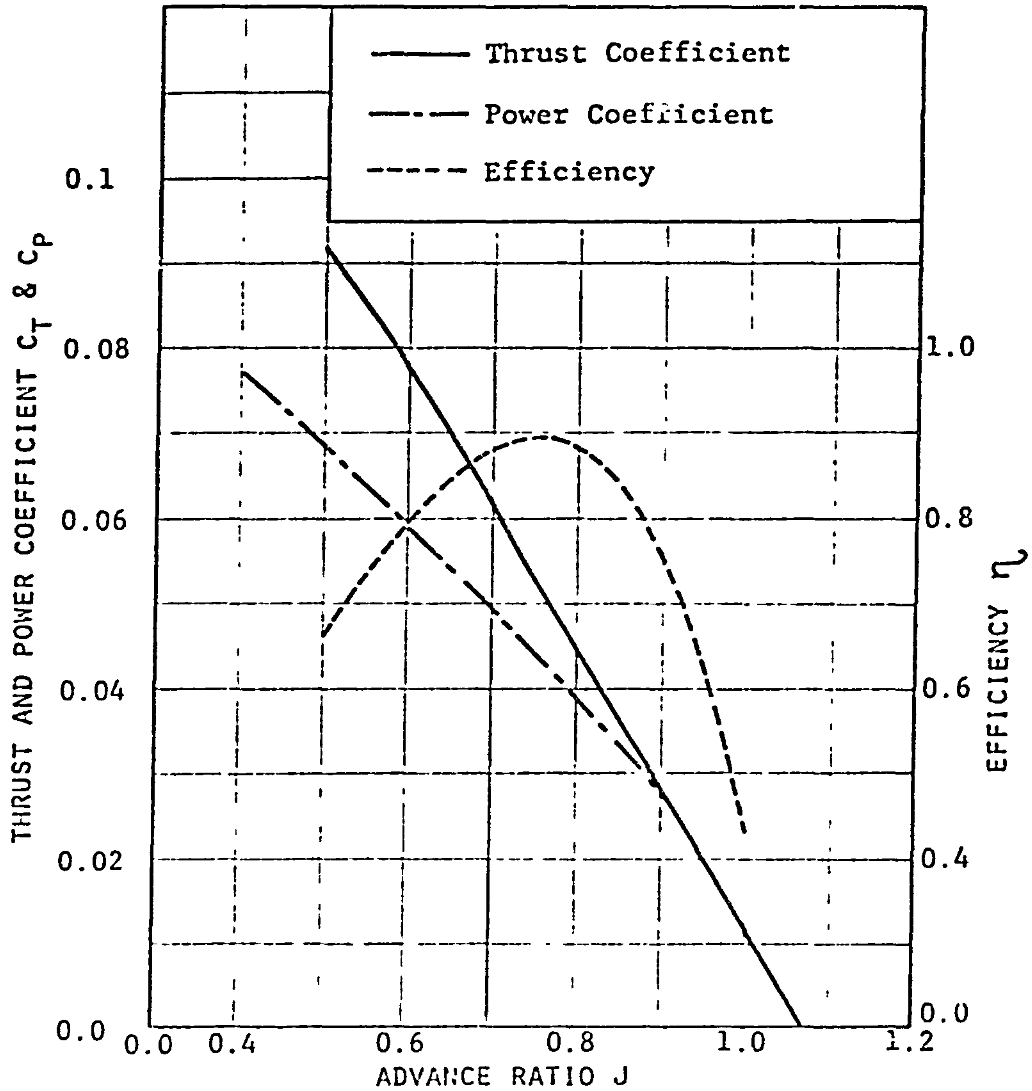

FIG. 15 PREDICTED STEADY STATE PERFORMANCE OF THE SENSENICH PROPELLER 76EM8-0-61

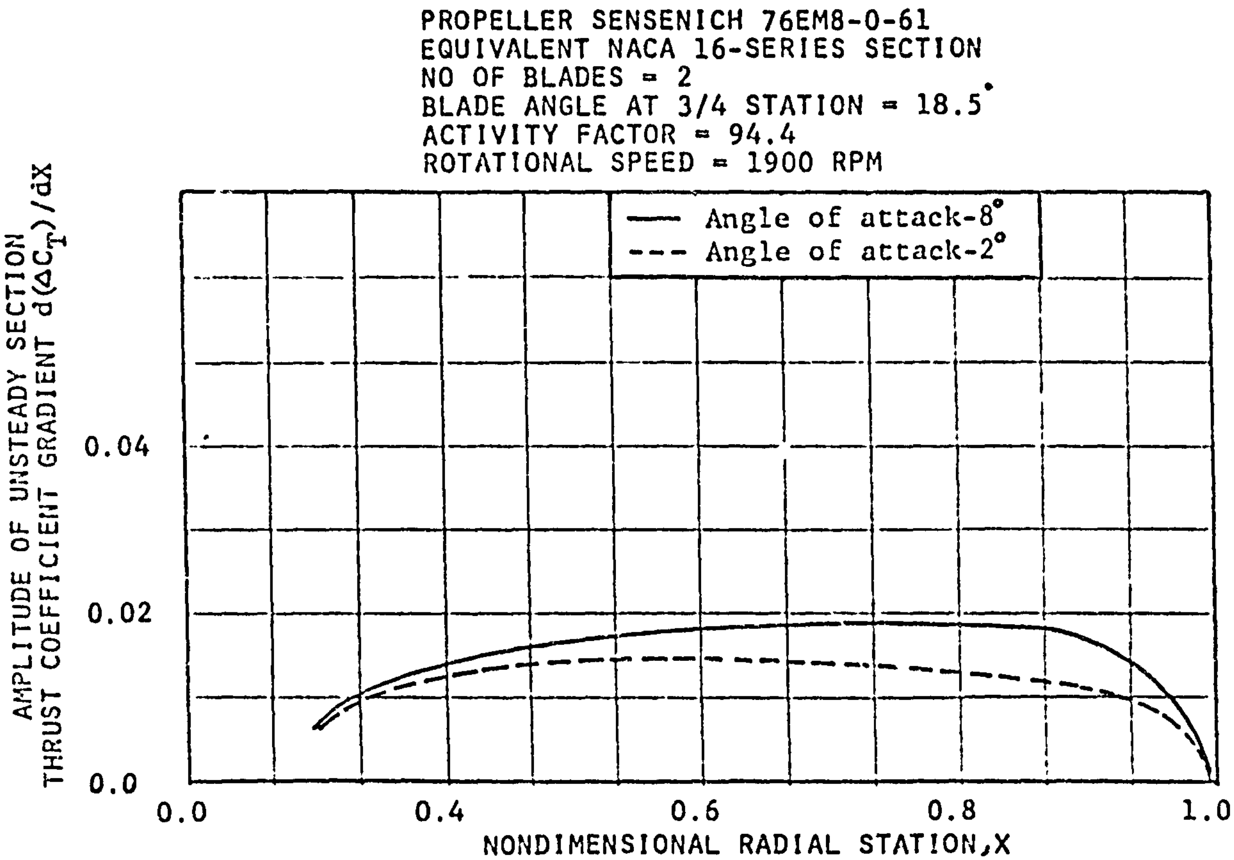

FIG. 16 DISTRIBUTION OF AMPLITUDE OF UNSTEADY SECTION THRUST COEFFICIENT GRADIENT FOR THE PROPELLER IN THE FLOW FIELD OF THE CHEROKEE 180

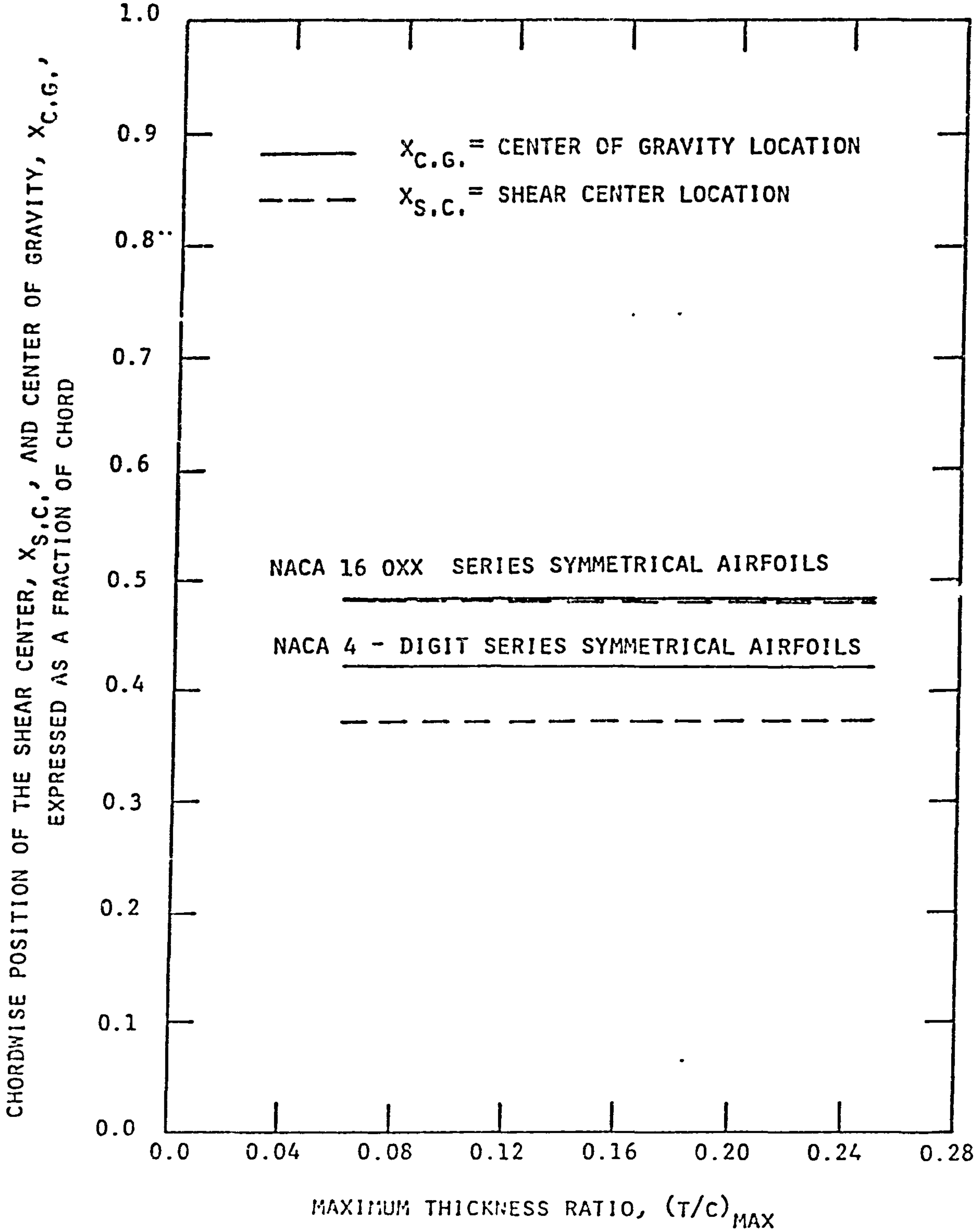

FIG. 17 SHEAR CENTER LOCATION FOR NACA 4-DIGIT SERIES VERSUS NACA 16 SERIES AIRFOILS

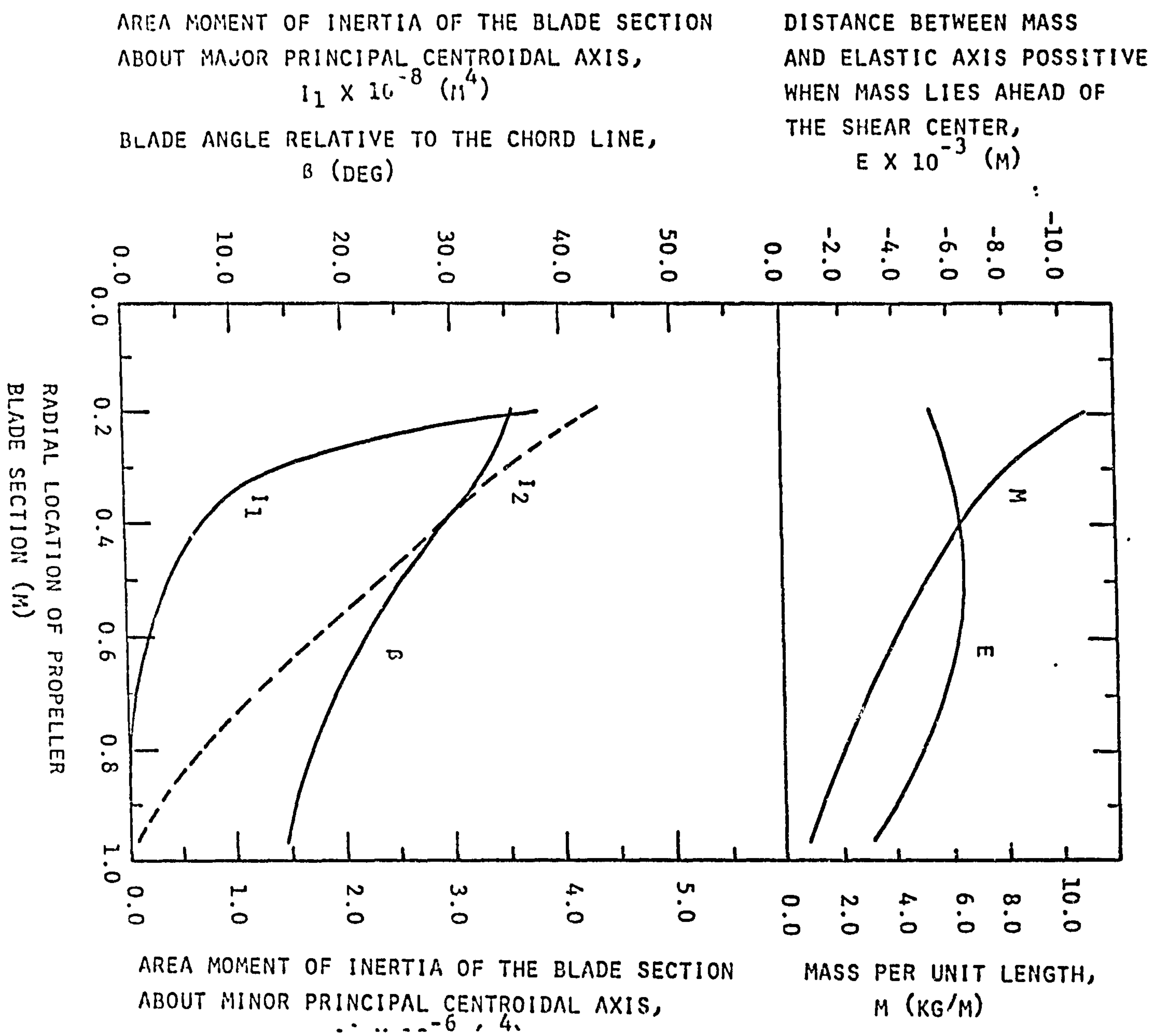

FIG. 18 MATERIAL AND GEOMETRICAL PROPERTIES OF A SENSENICH PROPELLER BLADE

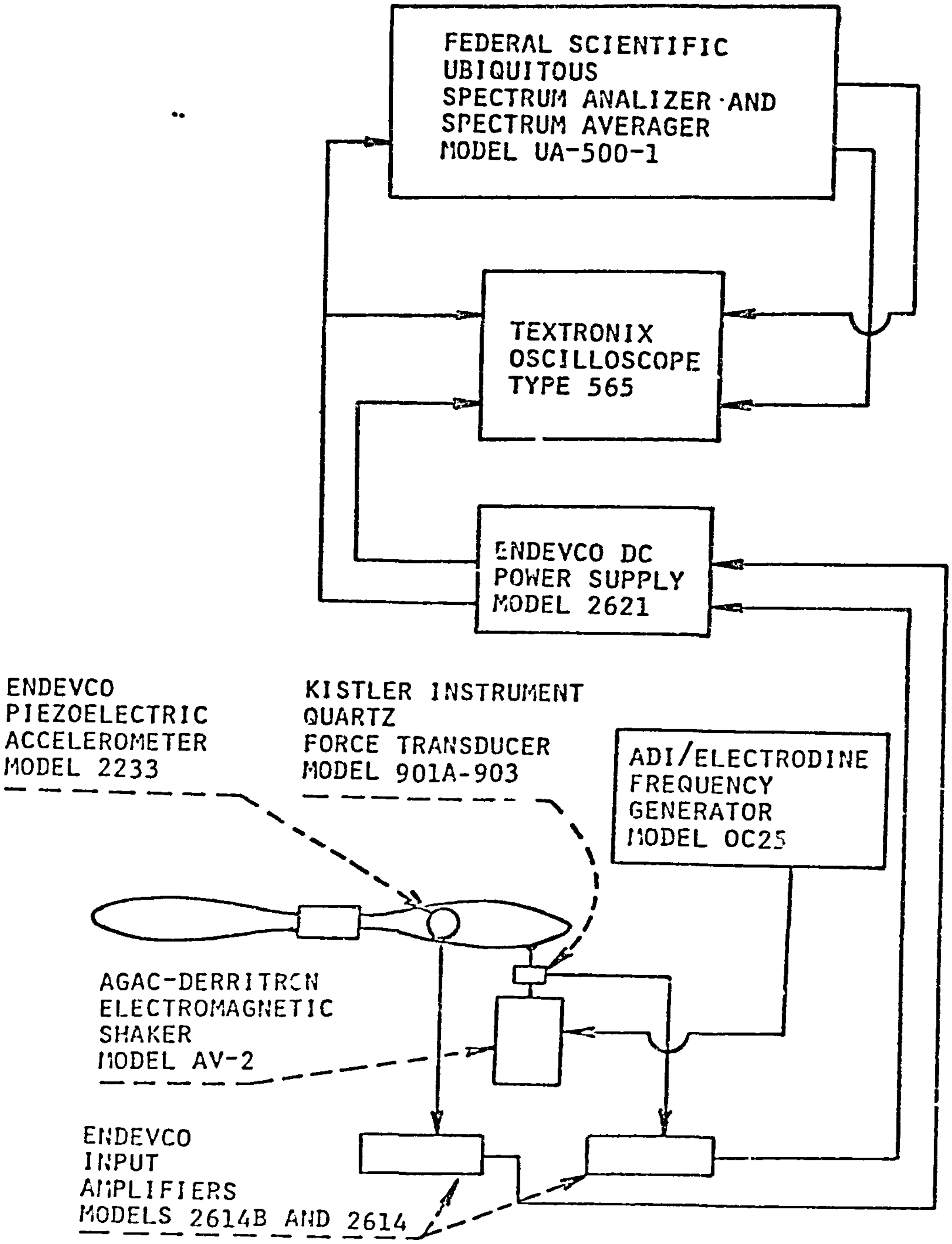

FIG. 19 SCHEMATIC OF TEST SETUP FOR DETERMINING PROPELLER BLADE NATURAL FREQUENCIES

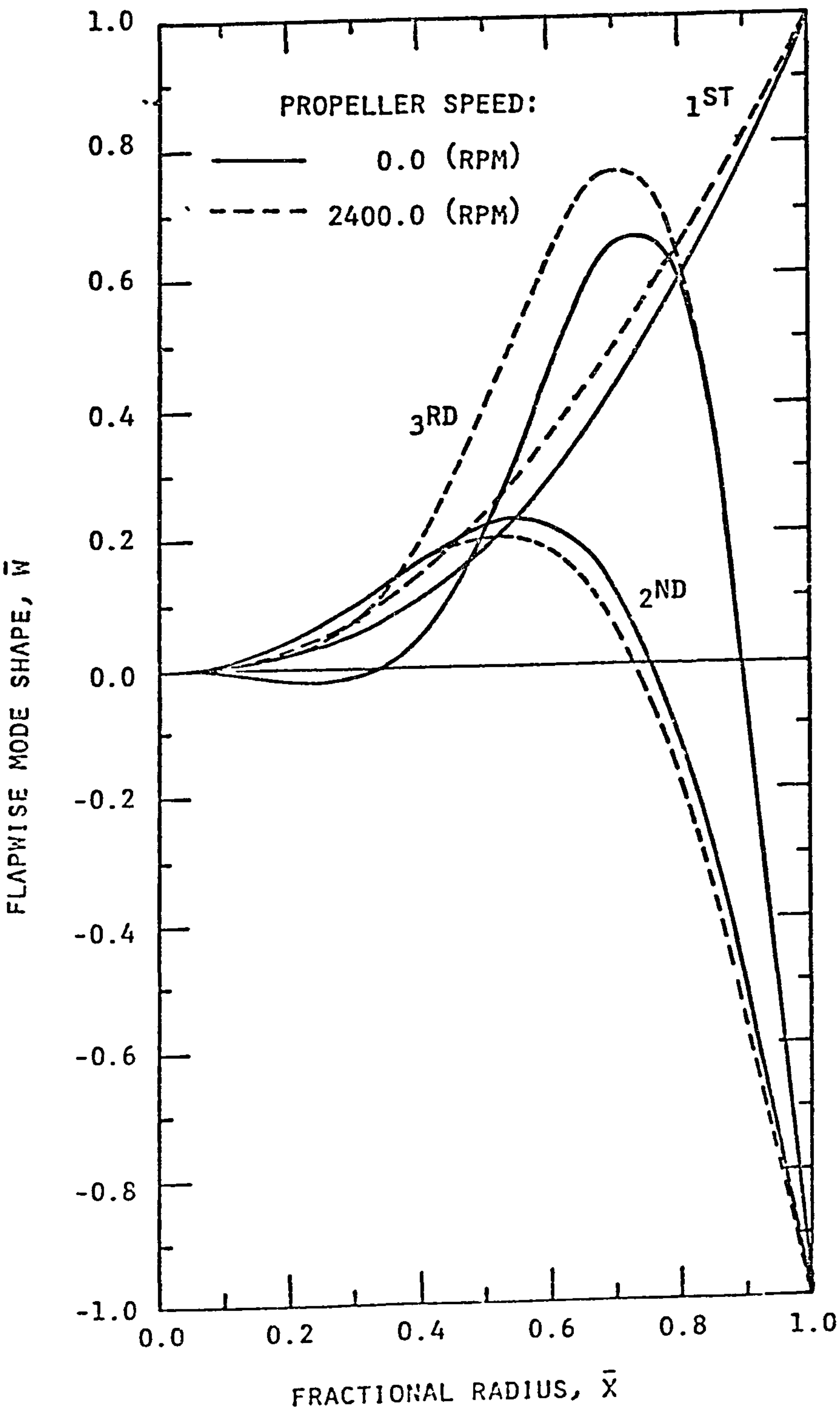

FIG. 20 PREDICTED MODE SHAPES OF COUPLED FLAPWISE BENDING AND CHORDWISE BENDING VIBRATIONS FOR A CLAMPED SENSENICH PROPELLER

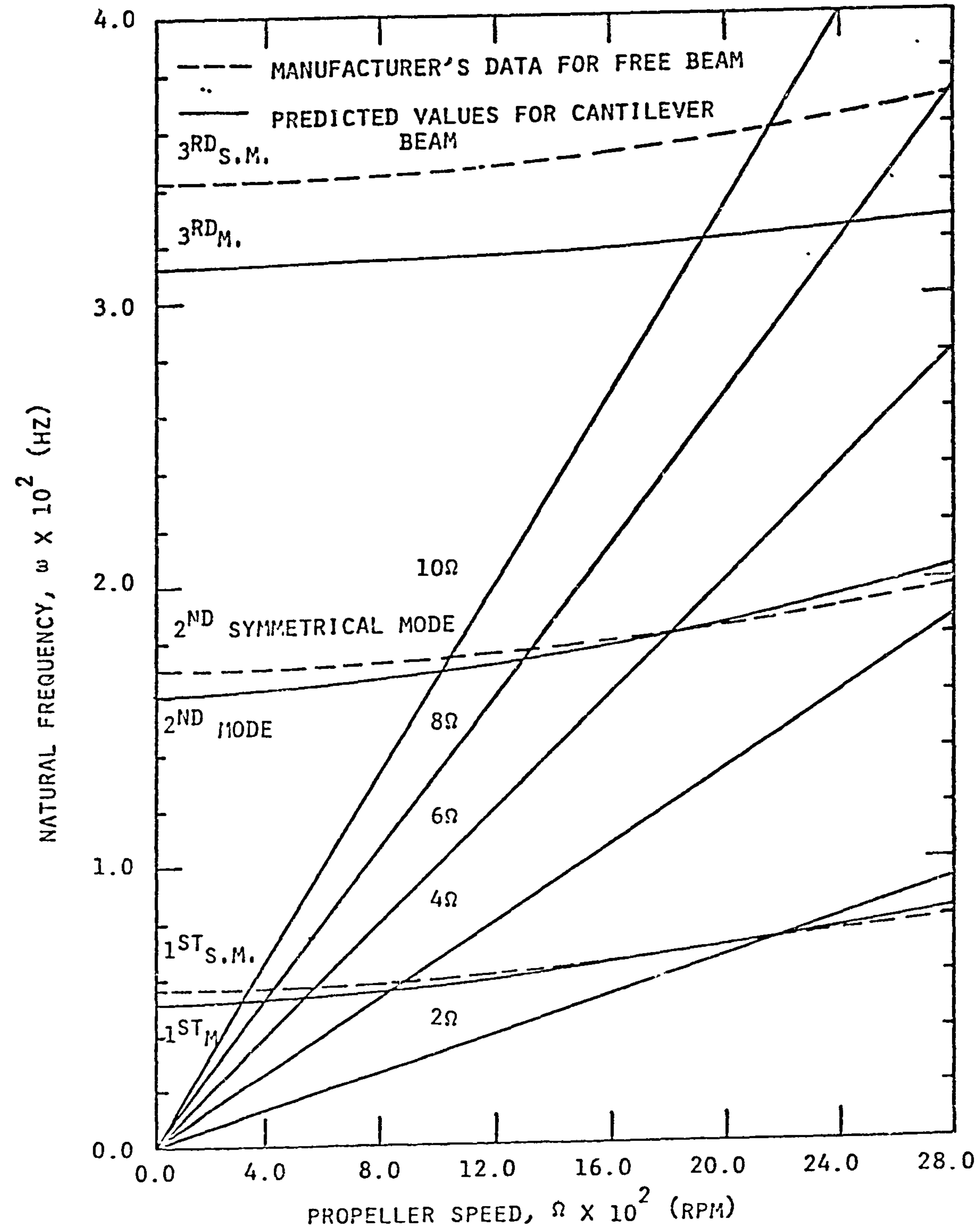

FIG. 21 PROPELLER NATURAL FREQUENCIES AND ENGINE EXCITING FREQUENCIES AS A FUNCTION OF PROPELLER SPEED

END

DATE

FILMED

APR 3 1979

End of Document